# Chapter 2

## Isolation, Total Synthesis, and Cytotoxic Activity of Compounds of *Ipomoea nil* Seeds

## 2. Isolation, total synthesis, and cytotoxic activity of compounds of *Ipomoea nil* seeds

### 2.1. Literature review

*Ipomoea nil* (L.) Roth (*Pharbitis nil* (L.) Choisy, Convolvulaceae), commonly known as morning glory, is an annual climbing herb used as a flowering plant (The Plant List, 2013). The genus *Ipomoea* comprises the largest genus of the family Convolvulaceae, consisting of about 500-600 species, and is widely distributed throughout the Southeast Asia. Its seeds are traditionally used as purgative in Korea, China, and Japan (Bensky and Gamble, 1993). The seeds have also been used as a folk medicine in Traditional Chinese Medicine as an analgesic for abdominal pain. *I. nil* seeds are well known to be rich in gibberellins and their glycosides (Yokota et al., 1971; Murofushi et al., 1968; Yokota et al., 1969; Tamura et al., 1967). Other than gibberellins, an array of diverse chemical constituents have been isolated from the *Ipomoea nil* seeds viz. allogibberic acid (Kim et al., 2013), monoterpene glycosides (Lee et al., 2017), phenylethanoid glycosides, phenylpropanoids (Kim et al., 2011), *ent*-kaurane diterpenoids and their glycosides (Kim et al., 2009; Woo et al., 2017; Lee et al., 2019), *ent*-gibbane diterpene glycoside (Kim et al., 2009), resin glycosides (Kawasaki et al., 1971; Li et al., 2017), phenolic amides (Kim et al., 2010), lignans (Kim et al., 2014; Kim et al., 2011), neolignans (Lee et al., 2017), triterpenoid saponins (Jung et al., 2008), fatty acid derivatives (Song et al., 2019), spermidine alkaloid (Schimming et al., 2005) (Figure 2.1).

The plant has been reported to have diverse pharmacological activities including antibacterial (Nguyen et al., 2017), antifungal (Koo et al., 1998), anti-inflammatory (Lee et al., 2017; Lee et al., 2019), antioxidant (Lee et al., 2019), cytotoxic (Kim et al., 2009; Song et al., 2020; Woo et al., 2017; Kim et al., 2010; Ko et al., 2004), α-glucosidase

inhibitory activity (Song et al., 2019), hepatoprotective (Oh and Chai, 2001), and multidrug resistance reversal activities (Li et al., 2017).

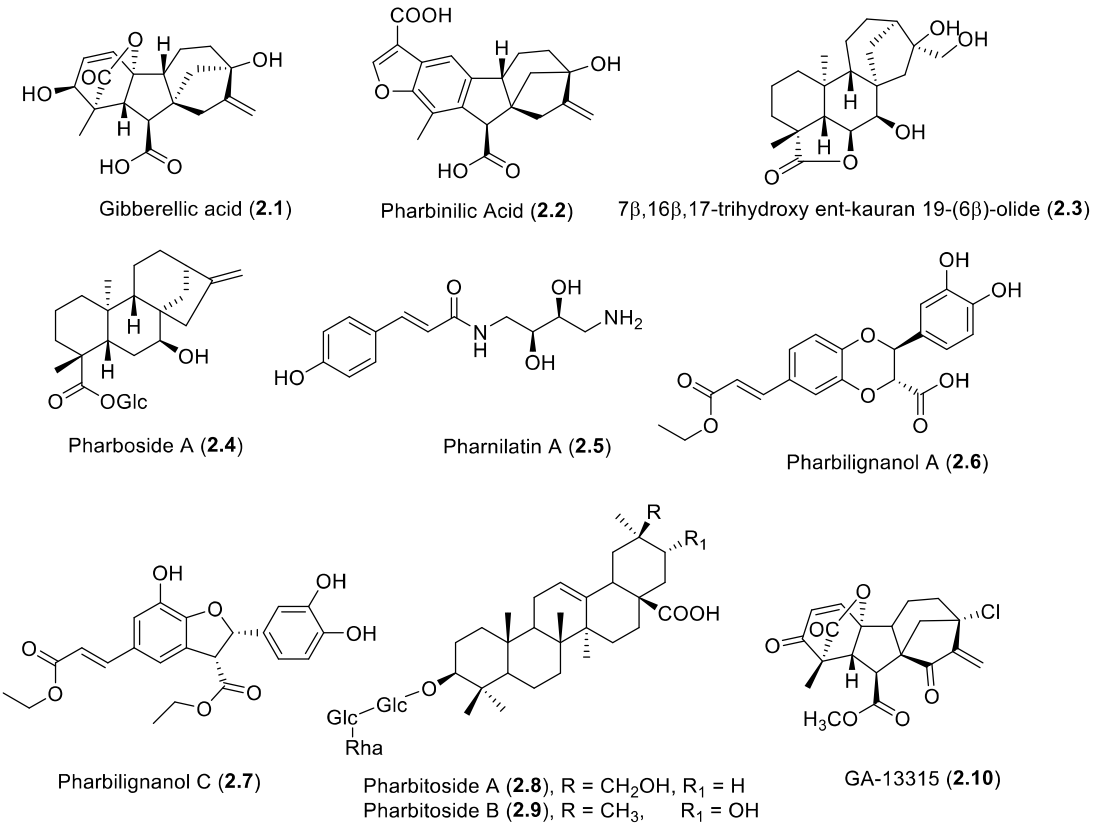


**Figure 2.1.** Chemical structures of compounds reported from *I. nil* (**2.1-2.9**) and semi-synthetic derivative GA-13315 (**2.10**)

*Ipomoea nil* has shown its anticancer potential in many *in-vitro* studies. The root extract of the plant is found to trigger apoptotic cell death of AGS gastric cancer cells in a dose- and time-dependent manner (Ko et al., 2004). The *ent*-kaurane diterpene glycosides isolated from *I. nil* seeds displayed moderate *in-vitro* cytotoxicity against five human tumor cell lines (Kim et al., 2009). Two phenolic amides, pharnilatins A and B, possessed cytotoxicity against human tumor cell lines (Kim et al., 2010). Lignans displayed anti-inflammatory activity and cytotoxicity against cancer cells (Kim et al., 2011; Kim et al., 2014). Resin glycosides (pharbatins) reversed multidrug resistance in

KB/VCR cells and also showed synergistic effects with vincristine (Li et al., 2017). Further, the seeds were shown to induce autophagy and apoptosis in lung cancer cells (Jung et al., 2017). Also, DA-9701 (Motilitone), a herbal formulation consisting of *Corydalis yanhusuo* (Papaveraceae) roots and *Pharbitis nil* seeds, has been used in the treatment of functional dyspepsia in Korea (Jin and Son, 2018). DA-9701 had completed six clinical trials (clinicalTrials.gov) for its global use.

Gibberellic acid and allogibberic acids are typical examples of gibbane-type diterpenes. They have been found in a variety of plants like *Malus domestica*, *Pisum sativum*, *Ipomoea* spp., *Prunus* spp., as well as microorganisms like *Gibberella fujikuroi* (fungus), *Acetobacter diazotropicus* (bacteria) (MacMillan, 2001; Mander, 2003). The gibberellin derivatives have shown promising biological activities, primarily anticancer (Zhu et al., 2020; Wu et al., 2018; Annand et al., 2015). GA-13315 (**2.10**, 13-chlorine-3,15-dioxy-gibberellic acid methyl ester), a gibberellin derivative, exhibited high antitumor and antiangiogenic activity *in vitro* and *in vivo* and displayed selectivity against multi-drug resistant MCF-7/ADR cells (Cheng et al., 2020). Thus, the gibberellic acid scaffold offers new chemical space to medicinal chemists for anticancer drug discovery. Since gibberellic acid (**2.1**, GA) is cheap and readily available, it could serve as a promising precursor for the synthesis of gibbane-type diterpenoids. Annand et al. (2015) synthesized an allogibberic acid previously isolated from *I. nil* seeds, pharbinilic acid (**2.2**) in 7 steps from GA. However, GA being a highly functionalized molecule with the strained ring, its reactivity poses inevitable challenges (Danheiser, 1984; Corey et al., 1978).

Based on the reported anticancer activity of *I. nil* seeds as well as compounds isolated from the same, we target this plant for the bioassay-guided isolation followed by

the screening of isolated compounds to identify the lead. Further, the lead was planned for synthetic or semi-synthetic modification to create a diverse compound library.

## 2.2. Results and discussion

### 2.2.1. Phytochemical investigation of *I. nil* seeds

A hydromethanolic ($H_2O$: Methanol, 2:8) extract of *I. nil* seeds was prepared under acidic conditions (by dil. HCl) and concentrated to evaporate methanol, which was subsequently fractionated with ethyl acetate to separate and enrich alkaloids and non-alkaloids respectively in aqueous and ethyl acetate fraction. The initial cytotoxicity study against HL60 cells showed the ethyl acetate fraction (containing non-alkaloidal content) to be active. The active fraction was concentrated and re-suspended in 1:9 methanol-water and allowed to pass through a column of polymeric HP20 resin. Adsorbed organic metabolites were then eluted by step gradient elution of increased content of methanol in water. Five fractions were pooled and further subjected to repeated silica gel column chromatography and Sephadex LH-20 based size-exclusion chromatography using hexane-ethylacetate and methanol respectively.

Eight compounds were isolated and characterized using 1D and 2D NMR spectroscopic and mass spectrometric analyses. Apart from one new compound (**2.11**), other known compounds viz. behenic acid (**2.12**) (Zheng et al., 2004), docosanol (**2.13**, behenyl alcohol) (Ajithabai et al., 2011), ester of ferulic acid with linear chain fatty alcohol i.e., tetracosyl ferulate (**2.14**) (Xiang et al., 2008), stigmasterol (**2.15**) (Forgo and Kövér, 2004), β-sitosterol (**2.16**) (Ododo et al., 2016), 7,3',5'-tri-*O*-methyltricetin (**2.17**) (Zahir et al., 1996), and apigenin (**2.18**) (Owen et al., 2003) were identified by comparing the observed NMR spectra with the reported spectroscopic data.

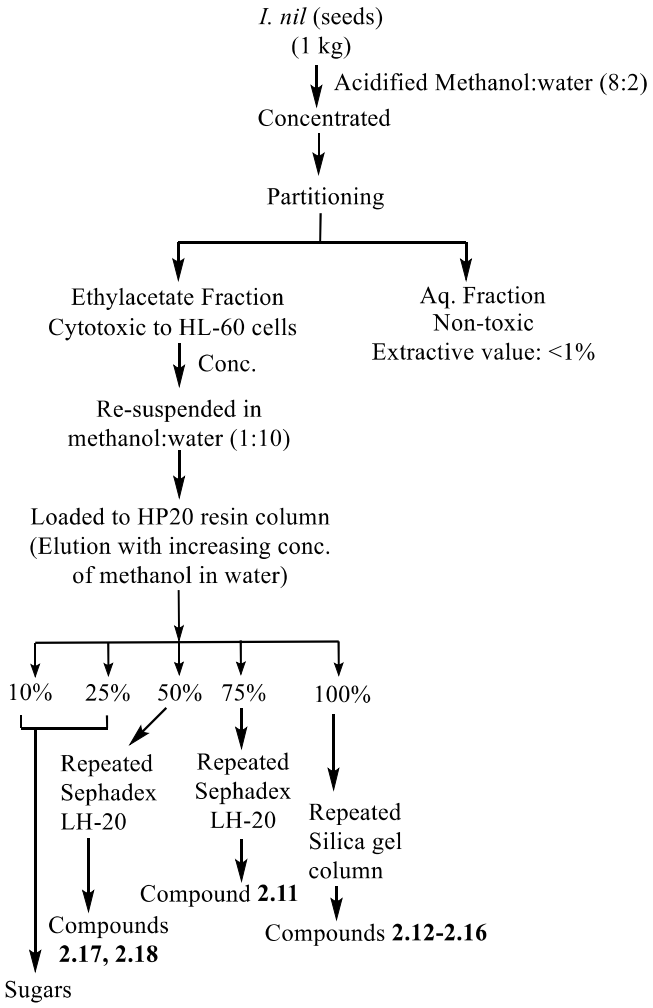


**Figure 2.2.** Schematic diagram of isolation of compounds **2.11-2.18** from *I. nil* seeds

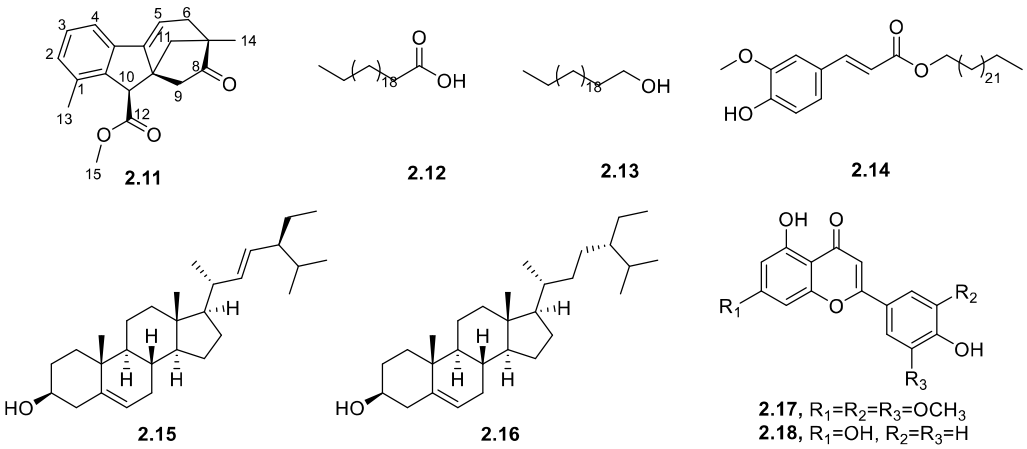


**Figure 2.3.** Chemical structures of compounds isolated from *I. nil* seeds

### 2.2.2. Structure elucidation of new compound 2.11

Compound **2.11** was isolated as an optically active, brown gummy mass, $[\alpha]_D^{19}$ +19 (*c* 0.40, $CHCl_3$), with molecular formula $C_{19}H_{20}O_3$ based on the HRMS (observed m/z $[M+H]^+$ 297.1487, calcd. for $C_{19}H_{21}O_3^+$, 297.1485) and detailed NMR data analyses (Table 2.1). The $^1H$ NMR spectrum (Figure 2.4) showed the presence of three aromatic protons at $\delta_H$ 7.29 (d), 7.21 (t), and 7.07 (d), one olefinic proton at $\delta_H$ 5.92 (t), one methoxy group at $\delta_H$ 3.70 (s), and one methyl group attached to the aromatic system at $\delta_H$ 2.24 (s). The $^{13}C$ NMR and DEPT-135 spectra (Figure 2.5) displayed two carbonyl groups at $\delta_C$ 219.9 and 172.2, eight olefinic carbons including four quarternary carbons between 148.8 and 114.0, and nine aliphatic carbons between $\delta_C$ 55.2 and 18.6 including one CH group at $\delta_C$ 55.2, one methoxy carbon at $\delta_C$ 51.9, three $CH_2$ carbons at $\delta_C$ 54.8, 42.1, 39.2, two methyl carbons at $\delta_C$ 20.7 and 18.6, and two quaternary carbons.

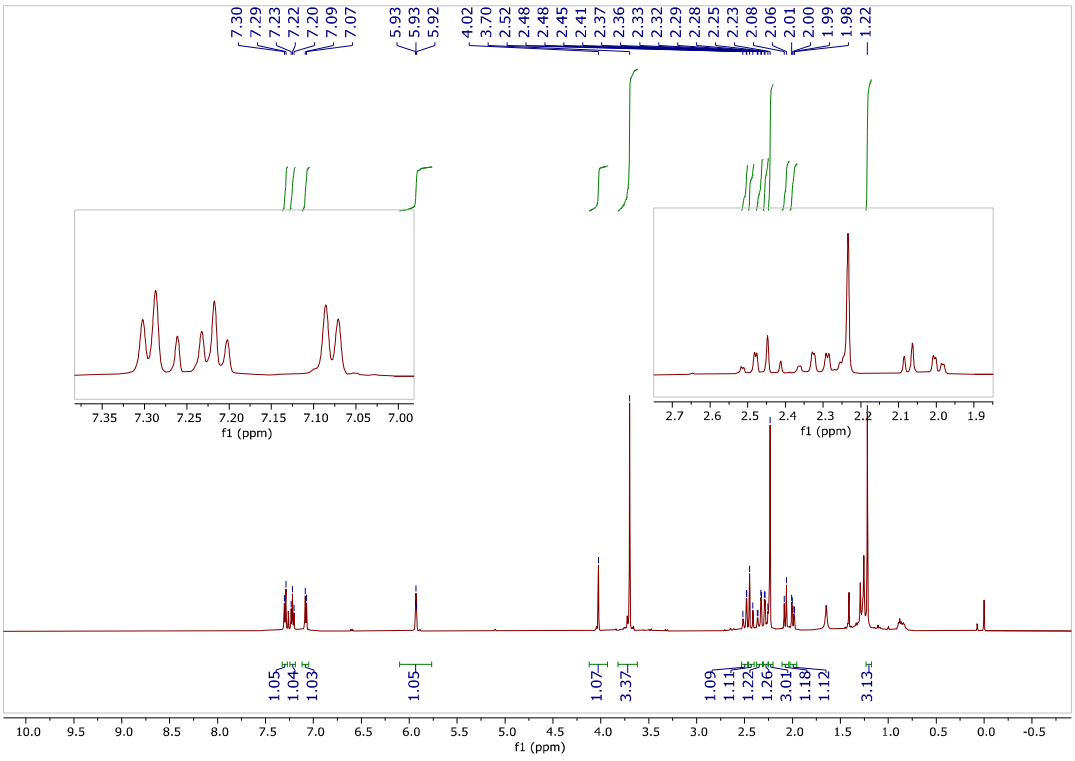


**Figure 2.4.** $^1H$ NMR spectrum of compound **2.11** in $CDCl_3$ (500 MHz)

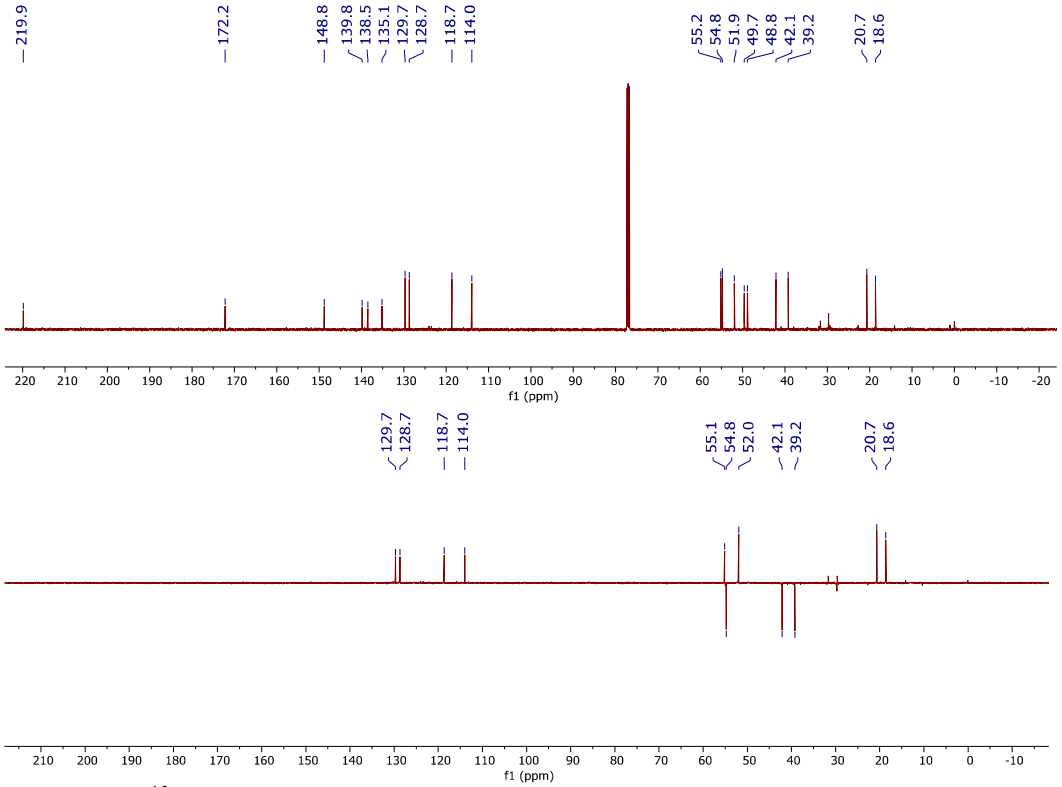


**Figure 2.5.** $^{13}C$ NMR and DEPT-135 spectra of compound **2.11** in $CDCl_3$ (125 MHz)

The COSY, HSQC, and HMBC spectra exhibited the following correlations. The olefinic proton at $\delta_H$ 7.21 ($\delta_C$ 128.7, C-3) showed $^1H$-$^1H$ COSY correlations to protons at $\delta_H$ 7.29 ($\delta_C$ 118.7, C-4) and 7.07 ($\delta_C$ 129.7, C-2). The methyl group at $\delta_H$ 2.24 ($\delta_C$ 18.6, C-13) showed three HMBC correlations to carbons at $\delta_C$ 129.7 (C-2), 135.1 (C-1), and 139.8 (C-10a), with C-2 and C-10a showing HMBC correlations to an olefinic proton at $\delta_H$ 7.29 ($\delta_C$ 118.7, C-4). The same proton ($\delta_H$ 7.29) showed another HMBC correlation to $\delta_C$ 138.5, C-4a. C-10a resonance also showed an additional HMBC correlation with an aliphatic proton at $\delta_H$ 4.02 ($\delta_C$ 55.2, C-10), which in turn possessed HMBC correlations with a carbonyl carbon at $\delta_C$ 172.2 (C-12) and carbon resonances at $\delta_C$ 48.8 (C-9a), 138.5 (C-4a). The C-12 resonance also showed a strong HMBC correlation to a methoxy group at $\delta_H$ 3.70 ($\delta_C$ 51.9, C-15), claiming the carbonyl group to be that of a methyl ester. C-4a resonance was also HMBC-correlated to an olefinic proton at $\delta_H$ 5.92 ($\delta_C$ 114.0, C-5)

which was subsequently correlated to carbon resonances at $\delta_C$ 148.8 (C-4b) and 48.8 (C-9a), along with a $^1$H-$^1$H COSY correlation to a methylene proton resonance at $\delta_H$ 2.29 ($\delta_C$ 39.2, C-6). These proton resonances showed HMBC correlations with carbon at $\delta_C$ 49.7 (C-7) and another carbonyl carbon at $\delta_C$ 219.9 (C-8). The C-7 carbon resonance was correlated to methylene proton resonance at $\delta_H$ 2.08 and 1.99 ($\delta_C$ 42.1, C-11), and a methyl proton resonance at $\delta_H$ 1.21 ($\delta_C$ 20.7, C-14). The carbonyl carbon (C-8) also showed HMBC correlation with methyl (C-14) protons and methylene protons at $\delta_H$ 2.45 ($\delta_C$ 54.8, C-9). Lastly, the HMBC correlations from the protons at $\delta_H$ 2.08 and 1.99 ($\delta_C$ 42.1, C-11), and 2.45 ($\delta_C$ 54.8, C-9) to C-9a were also observed. Based on these observations, the planar structure of compound **2.11** was determined as a bicyclo[3.2.1]octanone containing methyl 1,7-dimethyl-8-oxo-6,8,9,10-tetrahydro-7H-7,9a-methanobenzo[a]azulene-10-carboxylate.

The absolute configuration of **2.11** was determined by electronic circular dichroism (ECD) analysis and the NOESY spectrum. The ECD analysis has been used for the determination of stereochemistry of C-10 carboxylic acid in gibberic acids with an aromatic A ring based on a sign of cotton effect at around 230 nm region, independent of structural changes in the C/D and B/C ring junctions (Meguro et al., 1973). The ECD spectrum of **2.11** showed a similar ECD curve to those of the known corresponding compounds, which defined the *β*-configuration of the C-10 carboxyl group i.e. 10*R* absolute configuration (Figure 2.6a). Based on this established absolute configuration of C-10, the NOESY spectrum revealed the conformations of C-7 and C-9a stereocentres. NOE interactions were observed between H-10/H-11, H-11/H-14, and H-6/H-14 that confirmed the 7*R* and 9a*S* conformations (Figure 2.6b).

**Table 2.1.** $^{1}H$ and $^{13}C$ NMR spectroscopic data for new compound (**2.11**) in $CDCl_3$

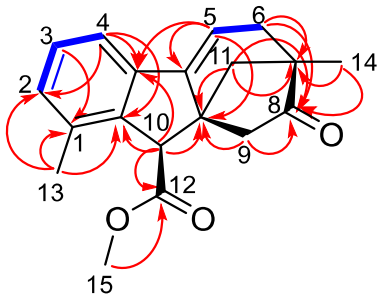


Key HMBC (red arrow) and $^{1}H$-$^{1}H$ COSY (bold blue line) correlations of compound **2.11**

| **Carbon No.** | $\delta_H$ | **mult (J in Hz)** | $\delta_C$ | **HMBC** |
|---|---|---|---|---|
| 1 | | | 135.1 (C) | |
| 2 | 7.07 | d (7.4) | 129.7 (CH) | |
| 3 | 7.21 | t (7.5) | 128.7 (CH) | C-1 |
| 4 | 7.29 | d (7.6) | 118.7 (CH) | C-2, 10a, 4a |
| 4a | | | 138.5 (C) | |
| 4b | | | 148.8 (C) | |
| 5 | 5.92 | t (3.0) | 114.0 (CH) | C-9a, 4a, 4b |
| 6 | 2.33 | m | 39.2 ($CH_2$) | C-7, 8 |
| 7 | | | 49.7 (C) | |
| 8 | | | 219.9 (C=O) | |
| 9 | 2.45 | m | 54.8 ($CH_2$) | C- 8, 9a |
| 9a | | | 48.8 (C) | |
| 10 | 4.02 | s | 55.2 (CH) | C-10a, 12, 9a, 4a |
| 10a | | | 139.8 (C) | |
| 11 | 2.08<br>1.99 | d (10.86)<br>dd (2.88, 10.84) | 42.1 ($CH_2$) | C-9a, 7, 8 |
| 12 | | | 172.2 (C=O) | |
| 13 | 2.24 | s | 18.6 ($CH_3$) | C-1, 2, 10a |
| 14 | 1.21 | s | 20.7 ($CH_3$) | C-7, 8 |
| 15 | 3.70 | s | 51.9($CH_3$) | C-12 |

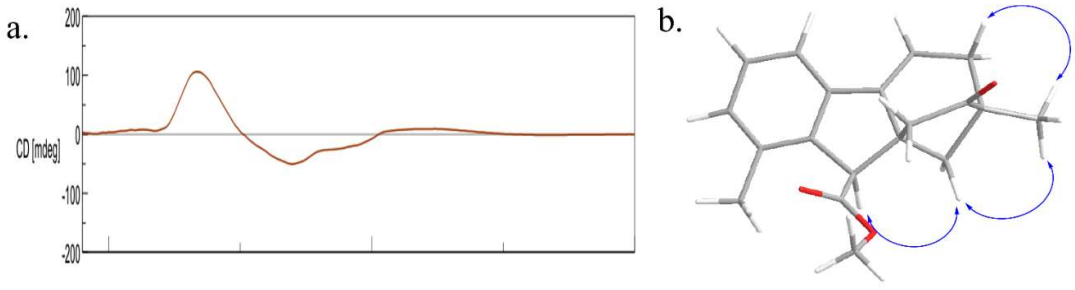


**Figure 2.6.** (a) ECD spectrum and (b) key NOESY correlations of compound **2.11**

Therefore, the absolute configuration of **2.11** was 7*R*, 9a*S*, and 10*R*. Thus the structure of compound **2.11** was elucidated as methyl (7*R*,9a*S*,10*R*)-1,7-dimethyl-8-oxo-6,8,9,10-tetrahydro-7H-7,9a-methanobenzo[a]azulene-10-carboxylate and was named as ipomone as shown in Figure 2.3.

### 2.2.3. Ipomone (2.11): An unusual bicyclo[3.2.1]octanone, perhaps a process generated product

The characteristic structural feature of ipomone is the presence of bicyclo[3.2.1]octanone instead of allylic alcohol of typical allogibberic compounds which are reported from *I. nil*. Bicyclo[3.2.1] octanone functionality in gibberic acids and related ent-kaurane diterpenoids has never been reported from any natural sources and it appears to be the first time. The literature search revealed that similar planar structure has been reported previously and was produced from gibberellic acid by synthetic reaction (Cross and Markwell, 1973). Structurally similar compound was also obtained during the total synthesis of pharbinilic acid from the gibberellic acid (Annand et al., 2015). Since, *I. nil* is a source of allogibberic compounds, we assumed ipomone as a process generated product. Perhaps, allylic alcohol containing allogibberic underwent acid-catalyzed 1,2 alkyl shift similar to pinacol-pinacolone rearrangement to produce corresponding bicyclo[3.2.1]octanone system.

Perhaps, the allylic alcohol containing substrate (**a**, in Figure 2.7) typically underwent an electrophilic substitution; hydroxylation under acidic conditions. Which normally led to the formation of 1,2-diol system (**b**); a representative of pinacol systems. Diol (**b**) may favor acid-catalyzed rearrangement, which is often called pinacol-pinacolone rearrangement. The characteristic feature of this rearrangement is that the protonated -OH group eases itself as a better leaving group and resulting carbocation

undergoes rearrangement by the shift of neighboring methyl group to give a stable molecule with a new carbon-oxygen double bond and led to the formation of (**c**); a representative of pinacolone system (Figure 2.7) (Annand et al., 2015). It is important to mention that the isolated compound **2.11** was obtained as a methylester, while, previous reported allogebberic acids have free carboxylic acid groups. Thus, esterification of acid with methanol being an acid-catalyzed process, it supports our hypothesis.

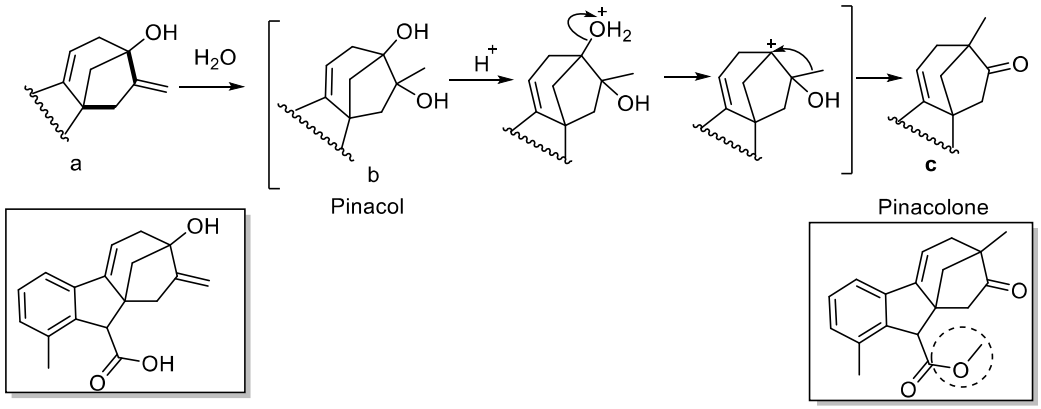


**Figure 2.7.** A plausible mechanism of 1,2 alkyl shift; a sort of pinacol-pinacolone rearrangement to produce **2.11.**

### 2.2.4. *In-vitro* anticancer activity of ipomone (2.11)

#### 2.2.4.1. Cytotoxicity of ipomone (2.11) against cancer cells

The novelty of ipomone (**2.11**) prompted us to investigate it for anti-cancer activity. It was evaluated for cytotoxicity against a panel of twelve human cancer cell lines, i.e., A549 (lung epithelial carcinoma), HL-60 (acute promyelocytic leukemia), MOLT-4 (acute lymphoblastic leukemia), MDA-MB-231 (breast adenocarcinoma), Hs579T (breast carcinoma), MCF-7 (breast carcinoma), PC-3 (prostate adenocarcinoma), OVCAR-3 (ovary epithelial carcinoma), HeLa (cervical epithelial carcinoma), MIA PaCa2 (pancreas epithelial cell carcinoma), HCT-116 (colorectal carcinoma), and HEK-293 (embryonic kidney), at the concentrations of 10, 20, 30, 40, 50, 60, 70, 80, 90, and

100 µM for 72 hours, using MTT assay (Guru et al., 2015). It exhibited weak cytotoxicity against all cell lines, except HEK-293 cells, with $IC_{50}$ values in the range of 34-86 µM after 48 hours (Table 2.2). The results revealed that A549 cells were the most sensitive cancer cells among all (A549, $IC_{50}$ 34.1 µM).

**Table 2.2.** Cytotoxicity of ipomone (**2.11)** against cell lines tested.

| S. No. | Tissue | Cell Line | $IC_{50}$± SD, µM, 48 h |
|---|---|---|---|
| 1 | Lung | A549 | 34± 1.011 |
| 2 | Blood | HL-60 | 48± 1.789 |
| 3 | Blood | Molt-4 | 42± 1.543 |
| 4 | Breast | MDA-MB-231 | 54± 1.997 |
| 5 | Breast | Hs579T | 59± 1.96 |
| 6 | Breast | MCF-7 | 66± 2.117 |
| 7 | Prostate | PC-3 | 53± 1.886 |
| 8 | Ovary | OVCAR-3 | 76± 2.432 |
| 9 | Cervix | HeLa | 66± 2.112 |
| 10 | Pancreatic | MIA-Pa-Ca-2 | 86± 2.912 |
| 11 | Colon | HCT-116 | 52± 1.117 |
| 12 | Kidney | HEK-293 | >100 |

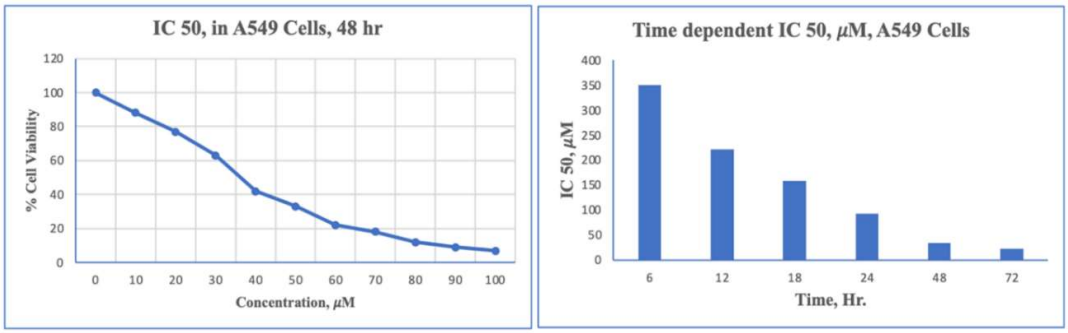


**Figure 2.8.** Dose and time dependent cytotoxicity of ipomone (**2.11**) against A549 cells.

### 2.2.4.2. Ipomone (2.11) causes A549 cell death by apoptosis

A dose/time-dependent cytotoxicity study was also performed on lung cancer A549 cells (Figure 2.9). DAPI (4′,6-diamidino-2-phenylindole) staining displayed that ipomone

caused chromatin condensation and DNA fragmentation, resulting in the formation of apoptotic bodies as visualized via fluorescence microscopy (Figure 2.9). Hence, proving that cytotoxicity is being mediated through induction of apoptosis and also proposes that this compound inhibits the growth of A549 cells by inducing apoptosis (Guru et al., 2015).

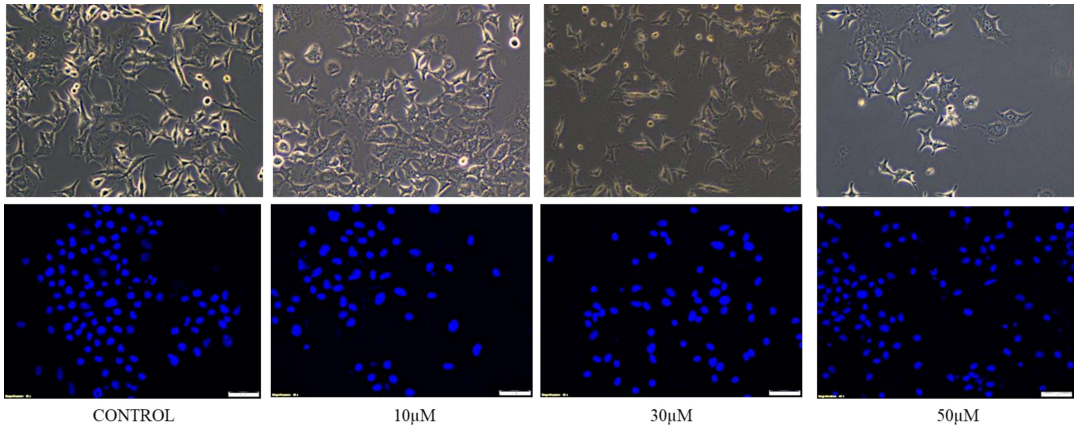


**Figure 2.9.** Fluorescence micrographs (DAPI staining) of A549 cells untreated and treated with ipomone for 24 hours. Ipomone (**2.11**) induced apoptosis in A549 cells.

### 2.2.4.3. Ipomone (2.11) induces autophagy

To confirm the autophagy inducing effect of ipomone, A549 cells were further examined in fluorescent micrographs after staining with acridine orange (AO) and propidium iodide (PI). As shown in Figure 2.10, cells treated with 10 and 30 μM of ipomone exhibited significant evidence of autophagy induction. The induction of autophagy increased in a dose-dependent manner (Kumar et al., 2013).

### 2.2.4.4. Immunoblot analysis

To confirm the above hypothesis, immunoblot analysis was performed for the apoptosis and autophagy genes. The expression levels of proteins involved viz. p110α, PARP-1, caspase-3, and LC-3 B were measured by western blot analysis after treatment with ipomone at 0, 10, 30, and 50 μM for 24hr. Ipomone displayed dose-dependent

induction of LC3B and decrease in PARP-1 and caspase-3 expression pattern as shown in Figure 2.11 (Guru et al., 2015).

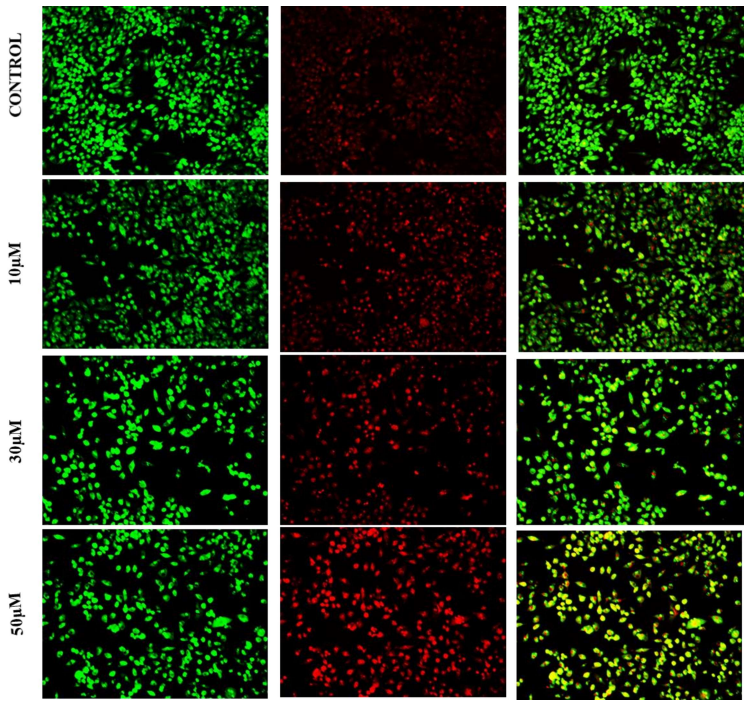


**Figure 2.10.** Morphology of untreated A549 cells (control) and those treated with 10, 30, and 50 μM of ipomone (**2.11**). Cells were stained by acridine orange (AO)/propidium iodide (PI) to study the autophagy inducing potential of ipomone.

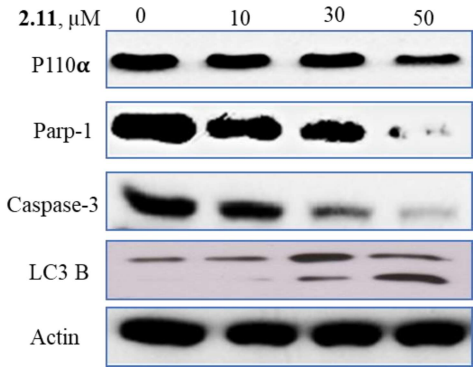


**Figure 2.11.** Immunoblot analysis using antibodies against the p110α, PARP-1, caspase-3, and LC 3B proteins in A549 cells after treatment with ipomone (**2.11**) (0-50 μM) for 24 hours

### 2.2.4.5. Molecular docking studies with caspase-3, p110α, and PARP-1 proteins

Upon successful completion of docking simulation best confirmation was selected with best binding energy in the largest cluster of 2.0 Å. The binding energy for ligand was found to be -7.39 Kcal/mol for caspase-3, -7.62 Kcal/mol for p110α, and -7.92 Kcal/mol for PARP-1. The ligands showed important interactions with the protein viz. H-bond, van der Waals, π-alkyl, π-π-stacked, and π-cation. The interactions of the ligand with caspase-3, p110α, and PARP-1 are represented in Figure 2.12.

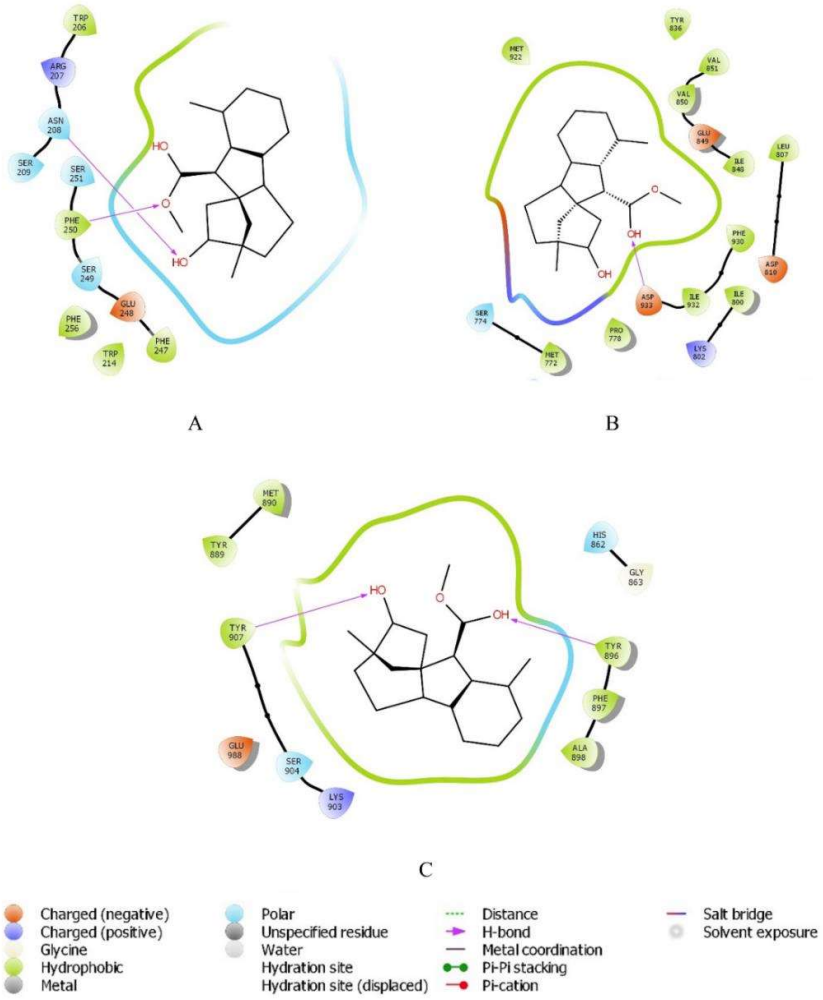


**Figure 2.12.** The protein-ligand interaction diagrams of ipomone with (A) caspase-3 (PDB id. 3KJF), (B) p110α (PDB id. 5DXT), and (C) PARP (PDB id. 6I8T)

### 2.2.5. Total synthesis of ipomone (2.11)

Ipomone (**2.11**) was assumed to be a process-generated product *via* an acid-catalyzed pinacol-pinacolone type of 1,2-alkyl shift because it was isolated from hydro-alcoholic extract under acidic conditions. So our next objective was to investigate the production of ipomone. Further, a sample of seed powder was subjected to hydro-alcoholic extraction under acidic, alkaline and neutral conditions. Ipomone was observed on TLC only in acidic extract. This prompted us to investigate the ipomone synthesis using gibberellic acid (GA) as a starting material under acidic condition. Gibberellic acid has been utilized earlier to synthesize pharbinilic acid (**2.2**) and a similar bicyclo[3.2.1]octanone was also obtained as by-product (Annand et al., 2015). So, we started our investigation by treating GA with different acids *viz.* HCl, HBr, HI, $H_2SO_4$, and $HNO_3$ in methanol and methanol-water (1:1) for 4 hours at room temperature, GA methyl ester was obtained as a major product (~90%) (entry 1-10, Table 2.3). Ipomone was visible on TLC as minor product (<10%) in case of HCl, HBr, and HI (entry 1-3, Table 2.3).

It is reported that electrophilic attack on the terminal alkene and the latent reactivity of tertiary hydroxyl group leads to several rearrangement reactions in GA (Hanson, 2018). Hence, the electrophiles were chosen to react with GA. $Br_2$ and $I_2$ was taken as an electrophile for the further investigations. When GA was subjected to react with bromine at room temperature for 4 hr in methanol, multiple products were visualized on TLC along with the desired compound **2.11** (entry 11, Table 2.3). Similarly, reaction with iodine produced compound **2.11** in a yield of ~40 % (entry 12, Table 2.3). Increasing the reaction temperature to 50 °C with 1 eq. of iodine in methanol resulted in a good yield of compound **2.11** (90%) within 2 hr (entry 13, Table 2.3, Figure 2.13). The compound was

purified with silica gel column chromatography and subjected to structural characterization. The spectroscopic properties of the isolated compound was same as ipomone (Goel et al., 2021).

**Table 2.3.** Treatment of gibberellic acid (**2.1**) under different reaction conditions

| Entry | Catalyst | Reaction conditions (Solvent/Time (hr)/Temp (°C) | Ipomone, yield (%) |
|---|---|---|---|
| 1 | HCl | Methanol/4/25 | <10 |
| 2 | HBr | Methanol/4/25 | <10 |
| 3 | HI | Methanol/4/25 | <10 |
| 4 | $H_2SO_4$ | Methanol/4/25 | - |
| 5 | $HNO_3$ | Methanol/4/25 | - |
| 6 | HCl | Methanol:Water (1:1)/4/25 | <10 |
| 7 | HBr | Methanol:Water (1:1)/4/25 | <10 |
| 8 | HI | Methanol:Water (1:1)/4/25 | <10 |
| 9 | $H_2SO_4$ | Methanol:Water (1:1)/4/25 | - |
| 10 | $HNO_3$ | Methanol:Water (1:1)/4/25 | - |
| 11 | $Br_2$ | Methanol/4/50 | Multiple products |
| 12 | $I_2$ (1 eq.) | Methanol/4/25 | ~40% |
| 13 | $I_2$ (1 eq.) | Methanol/2/50 | Ipomone (**2.11**) 90 % |
| 14 | $I_2$ (2 eq.) | Methanol/2/50 | **2.11** (60 %) |
| 15 | $I_2$ (2 eq.) | Methanol/4/50 | **2.19** (90 %) |
| 16 | $I_2$ (2 eq.) | Ethanol/4/50 | **2.20** (90 %) |

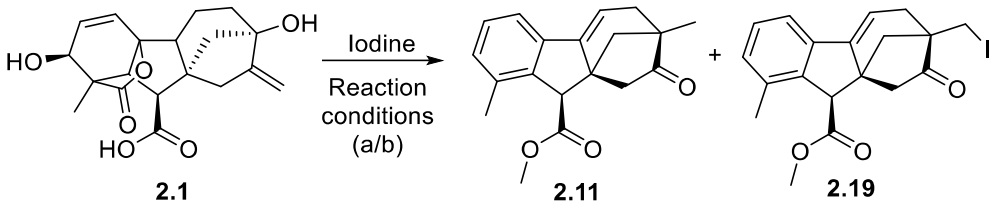


**Figure 2.13.** Chemical reaction of gibberellic acid (**2.1**) with iodine to synthesize ipomone (**2.11**). Reaction conditions: a) $I_2$ (1 equiv.), methanol (2 mL), 50 °C, 2 hr, yield (**2.11**: 90%, **2.19**: 0%). b) $I_2$ (2 equiv.), methanol (2 mL), 50 °C, 4 hr, yield (**2.11**: 5%, **2.19**: 90%).

However, when two or more equivalent of iodine was used, the yield of compound **2.11** decreased to 60 %, and a new product (**2.19**) appeared in a significant amount (yield 35%) within 2 hours (entry 14). Prolonging the reaction time to 4 hr at 50 °C resulted in the synthesis of compound **2.19** with the increased yield of 90 % (entry 15, Table 2.3, Figure 2.13). Compound **2.19** was purified by silica gel column chromatography and characterized by 2D NMR (Table 2.4) and HRMS. The $^{1}$H-NMR and $^{13}$C-NMR were identical to that of ipomone, except for an aliphatic $CH_3$ corresponding to $\delta_H$ 1.22 ppm and $\delta_C$ 20.7 ppm. An extra peak of $CH_2$ was also observed in the $^{13}$C NMR spectrum (confirmed by DEPT-135) at $\delta_C$ 10.4 ppm and corresponding peaks in $^{1}$H NMR at 3.50 and 3.34 ppm. The $CH_2$ peak at $\delta_C$ 10.4 ppm was highly shielded because of the substitution of electrophile-iodine ($CH_2I$). Further, the 2D NMR and HRMS data supported the formation of compound **2.19** i.e., methyl (7*S*,9a*S*,10*R*)-7-(iodomethyl)-1-methyl-8-oxo-6,8,9,10-tetrahydro-7H-7,9a-methano-benzo[a]azulene-10-carboxylate (**2.19**). The iodinated derivative **2.19** was obtained only when excess of iodine was used in the reaction. To evaluate the role of methanol in esterification of carboxylic group, the same reaction was carried out in ethanol (in place of methanol), this resulted in the formation of ethyl ester (**2.20**) (entry 16, Table 2.3). This proved the participation of methanol/ethanol in the esterification of carboxylic acid functionality.

### 2.2.5.1. Mechanism of formation of ipomone from gibberellic acid

To establish the plausible mechanism of the reaction, we collected and analysed an aliquot during the reaction. Immediately the reaction mixture was subjected to preparative TLC to isolate two intermediates **2.11a** and **2.11b** (Figure 2.16). When intermediate **2.11a** was analysed by NMR, it was found that the $^{13}$C NMR peak at 215.8 ppm appeared due to the formation of a carbonyl group. At the same time, peaks for exocyclic double bond

**(a)**

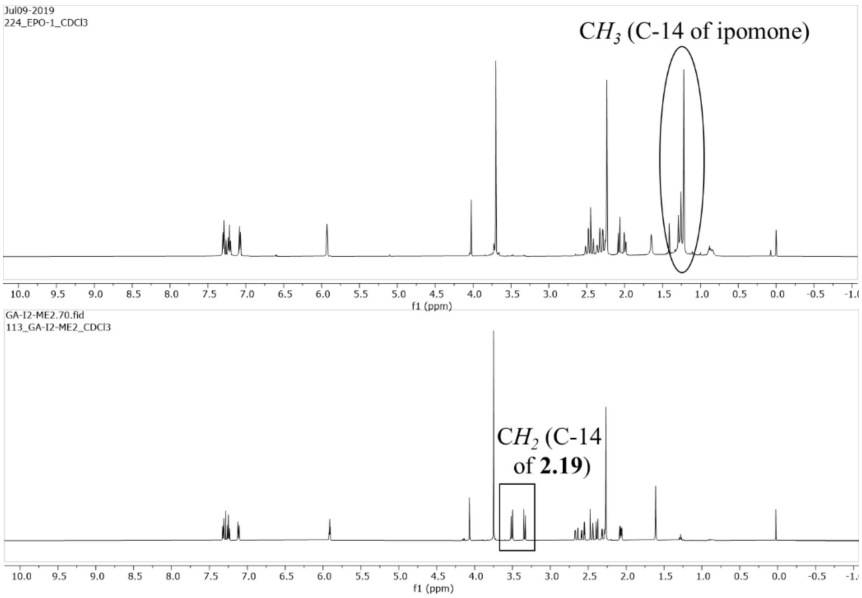


**(b)**

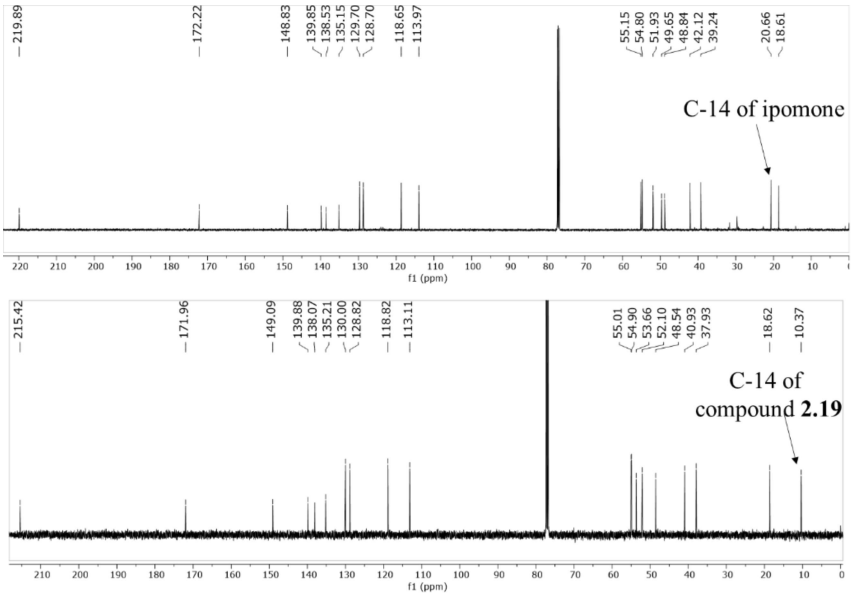


**(c)**

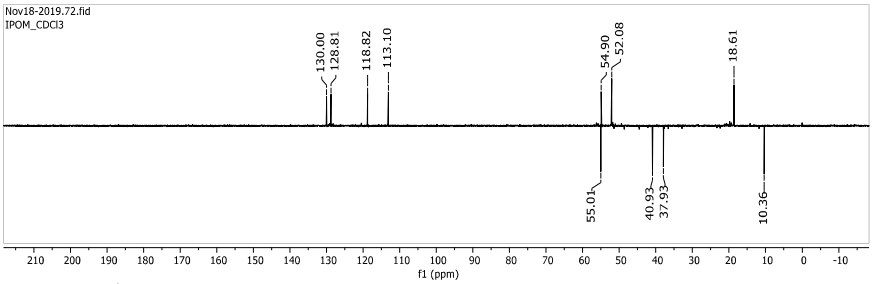


**Figure 2.14.** (a) $^{1}$H NMR spectra of ipomone and compound **2.19** in $CDCl_3$ (500 MHz); (b) $^{13}$C spectra of ipomone and compound **2.19** in $CDCl_3$ (125 MHz); (c) DEPT-135 NMR spectrum of compound **2.19** in $CDCl_3$ (125 MHz)

**Table 2.4.** $^{1}H$ and $^{13}C$ NMR spectroscopic data for compound **2.19** in $CDCl_3$.

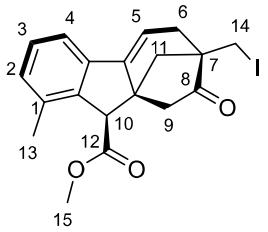


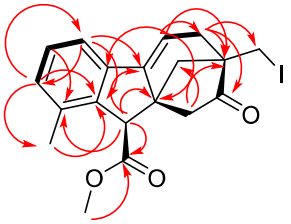


Key HMBC (red arrow) and $^{1}H$-$^{1}H$ COSY (bold black line) correlations

| Carbon No. | $\delta_H$ | mult ($J$ in Hz) | $\delta_C$ | HMBC |
|---|---|---|---|---|
| 1 | | | 135.2 (C) | |
| 2 | 7.11 | d (7.4) | 130.0 (CH) | C-13, 10a, 4 |
| 3 | 7.24 | t (7.5) | 128.8 (CH) | C-1 |
| 4 | 7.31 | d (7.6) | 118.8 (CH) | C-2, 4b, 10a |
| 4a | | | 138.1 (C) | |
| 4b | | | 149.1 (C) | |
| 5 | 5.91 | t (3.5) | 113.1 (CH) | C-6, 7, C-9a, 4a |
| 6 | 2.65 | dd (18.1, 3.0) | 37.9 ($CH_2$) | C-7, 8, C-14, 5, 4b |
| | 2.31 | d (3.9) | | |
| 7 | | | 53.7 (C) | |
| 8 | | | 215.4 (C=O) | |
| 9 | 2.56 | dd (17.3, 3.5) | 55.0 ($CH_2$) | C-11, 8, 9a, 4b, 7 |
| | 2.45 | d (17.4) | | |
| 9a | | | 48.5 (C) | |
| 10 | 4.06 | s | 54.9 (CH) | C-10a, 12, 9a, 4b, 1 |
| 10a | | | 139.9 (C) | |
| 11 | 2.38 | d (11.0) | 40.9 ($CH_2$) | C-9a, 7, 8 , 6 |
| | 2.07 | dd (8.2, 2.8) | | |
| 12 | | | 172.0 (C=O) | |
| 13 | 2.26 | s | 18.6 ($CH_3$) | C-1, 2, 10a |
| 14 | 3.50 | d (10.3) | 10.4 ($CH_2$) | C-11, 7, 8, 6 |
| | 3.34 | d (10.4) | | |
| 15 | 3.74 | s | 52.1 ($CH_3$) | C-12 |

(in ring D) at 157.0 ppm and 106.6 ppm disappeared. A peak also appeared at 10.3 ppm that is due to $CH_2I$ group (confirmed by DEPT-135). However, in this intermediate, NMR peaks were not observed in the aromatic region. This data concludes the formation of iodomethyl group as well as bicyclo[3.2.1]octanone, even before the aromatization of ring A. Owing to the unstability of this intermediate, it couldn't be characterized completely. While in another intermediate **2.11b**, we observed that the aromatic system was formed in ring A, but 1,2-alkyl rearrangement was not observed in rings C/D. This

investigation supports that both aromatization of ring A and 1,2-alkyl shift/rearrangement took place simultaneously.

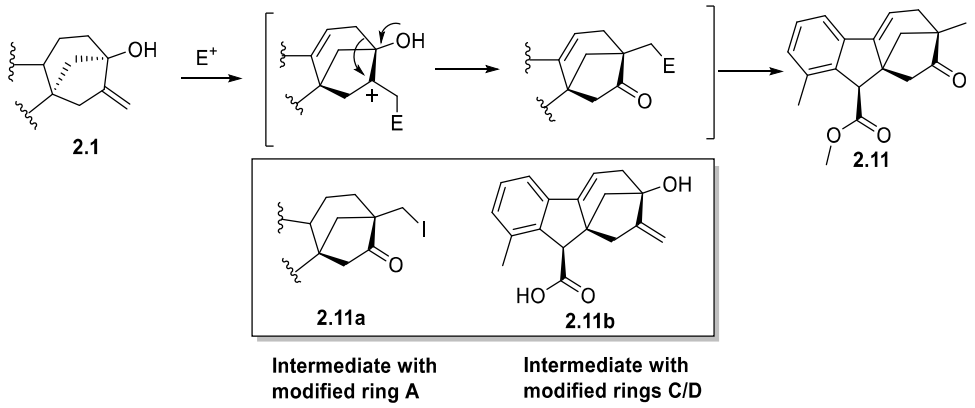


**Figure 2.15.** A plausible mechanism involved in the synthesis of ipomone (**2.11**). ($E^+$ for electrophile)

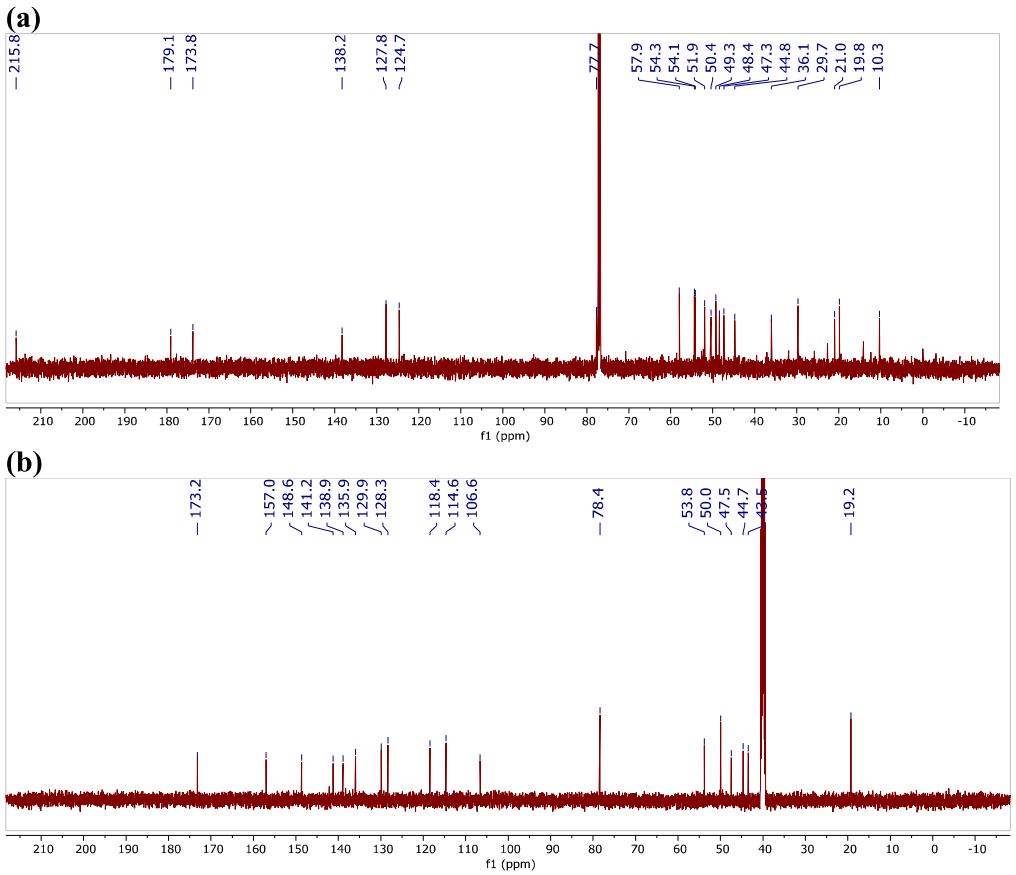


**Figure 2.16.** $^{13}C$ NMR spectra of intermediates (a) **2.11a** and (b) **2.11b** in $CDCl_3$ (125 MHz)

Four major modifications happened in the entire process viz. deacarboxylation, aromatization of ring A, esterification, and 1,2-alkyl rearrangement in rings C/D. Molecular iodine is a versatile catalyst for the oxidative aromatization of unsaturated carbonyl compounds and several protocols have been reported for the same (Mphahlele, 2009). The reaction was conducted in a protic solvent (methanol); therefore, it is possible that the protic solvent induced HI generation. The acidic conditions facilitated the elimination of lactone, decarboxylation, and dehydration, and is followed by iodine promoted aromatization to produce fully aromatized ring A.

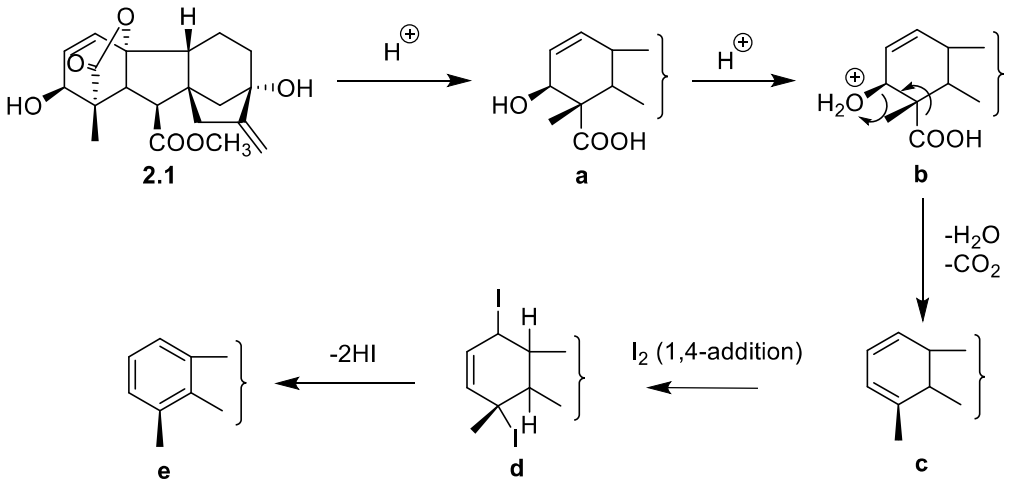


**Figure 2.17.** Plausible mechanism for the aromatization of ring A

Plausible mechanism of aromatization includes the hydrolysis of C1-C4a lactone bridge (intermediate **a**), followed by decarboxylation and dehydration to generate a cyclohexadiene ring system (intermediate **c**). The cyclohexadiene then forms a 1,4-iodine adduct (intermediate **d**) that undergo elimination of HI to form aromatic ring A (Figure 2.17) (Mphahlele et al., 1996).

Iodine being an electrophile, has also been used for the aromatization of terpenoids due to its rapid reactivity with unsaturated systems (Domingo et al., 2016; Singh et al., 2019). 1,2-alkyl rearrangement in rings C/D may have been proceeded *via* acid-catalyzed

pinacol−pinacolone type 1,2 alkyl shift, as reported previously (Goel et al., 2021). Further the unsaturation in ring C (C4b-C5 double bond) might be due to iodine-mediated addition and elimination reactions. Iodine also mediated the esterification; hence, the methyl ester was obtained from iodine-methanol. In the present work, the aromatization and 1,2-alkyl rearrangement occurred simultaneously to produce bicyclo[3.2.1]octanone containing ipomone in one step. Furthermore, the stipulated reason for compound **2.19** could be the formation of *in-situ* HI that reacts with ipomone (**2.11**) and produce **2.19** as a side product. To evaluate the role of methanol in esterification of carboxylic group, the same reaction was carried out in ethanol (in place of methanol), this resulted in the formation of ethyl ester (**2.20**) (entry 16, Table 2.3). This proved the participation of methanol/ethanol in the esterification of carboxylic acid functionality.

## 2.3. Experimental section

### 2.3.1. General experimental procedures

All chemicals were purchased from Sigma Aldrich and used as received. Optical rotation was measured on JASCO P-2000 polarimeter. The 1D and 2D NMR spectra were recorded on Bruker-Avance III HD 500 MHz NMR spectrometer using tetramethylsilane (TMS) as the internal standard and are referenced to the residual proton/carbon in the NMR solvent ($CDCl_3$, 7.26/77.1 ppm; DMSO-$d^6$, 2.50/39.5 ppm). The ECD spectrum was measured on a JASCO J-1500 spectropolarimeter. ESI-MS and HRMS spectra were recorded on Agilent 1100LC-QTOF and HRMS-6540-UHD spectrometers. The UV spectrum was recorded on Cary 60 UV–Vis spectrophotometer (Agilent Technologies). IR spectra were recorded on Perkin-Elmer IR spectrophotometer. All chromatographic purifications were performed on Dianion HP20 (Sigma), Sephadex LH20 (Sigma), silica gel (#60–120 or #100–200) obtained from Merck. The thin-layer chromatography (TLC)

was performed on pre-coated silica gel 60 GF254 aluminium sheets (Merck) and visualized under UV light (254 nm) and by spraying anisaldehyde-sulphuric acid reagent followed by heating.

### 2.3.2. Plant material

The seeds of *Ipomoea nil* were obtained from the local market of Varanasi, India, in March 2019, and authenticated by Prof. Nawal Kishore Dubey, Centre of Advanced Study in Botany, Institute of science, Banaras Hindu University, Varanasi. A specimen sample (voucher number, Convolvula, 2020/1) was preserved in the herbarium.

### 2.3.3. Extraction and isolation

The seeds of *I. nil* (1 kg) were coarsely powdered and extracted with acidified methanol-water (80:20, 1.5 L x 2, each for 48 hours) at room temperature. The hydro-alcoholic extract was concentrated to evaporate alcohol, and the remaining aqueous portion was portioned with ethyl acetate. Ethylacetate fraction was concentrated to get 6.4 gm fraction that was again re-suspended in 9:1 water-methanol (200 mL) and loaded to HP20 resin (10 mL, 5 % v/v) in a glass column. A pre-activated HP-20 resin (soaked in methanol overnight) was loaded in a glass column and equilibrated with distilled water. The extract was loaded to the resin column and allowed to settle down for some time. The adsorbed material was eluted with methanol in a gradient manner increasing from 100% distilled water to 100% methanol. Total 5 fractions were collected (each 50 mL except Fr 1: 200 mL) at the gradient elution of increasing methanol in water; Fr 1: 100% water, Fr 2: 75% water, Fr 3: 50% water, Fr 4: 25% water, and Fr 5: 100% methanol. Fr 1 and 2 were loaded with highly polar primary metabolites like sugar. Fr 3 was subjected to repeated sephadex LH-20 based size exclusion chromatography in methanol, and compounds **2.17** and **2.18** were obtained as pure compounds and characterized as tri-O-

methyltricetin and apigenin, respectively. Fr 4 yielded compound **2.11** after repeated sephadex LH-20. Fr 5 contained mainly lipophilic metabolites and compounds **2.12-2.16** were purified after repeated silica gel column chromatography in hexane-ethyl acetate gradient. Novel metabolite **2.11** was identified as *Ipomone* based on detailed 2D NMR and compounds **2.12-2.17** were identified by comparing the observed NMR spectra with the reported spectroscopic data.

**Ipomone (2.11):** The compound is a light brown gummy solid; 15 mg; $[\alpha]_D^{19}$ +19 (*c* 0.40, $CHCl_3$); UV (MeOH) $\lambda_{max}$ (log $\varepsilon$) 205 (4.11), 259 (3.33), 270 (3.27), 288 (3.02), 300 (2.96) nm; ECD (MeOH) $\lambda_{max}$ 234, 269 nm; IR (KBr) $\nu_{max}$ 2345, 2130, 1638, 1618, 1384, 1352, 618 $cm^{-1}$; $^1H$ NMR (500 MHz, $CDCl_3$) and $^{13}C$ NMR (125 MHz, $CDCl_3$) data, see Table 2.1; ESIMS *m/z* 297.30 $[M+H]^+$; HRMS m/z 297.1487 $[M+H]^+$ (calcd. for $C_{19}H_{21}O_3^+$, 297.1485) (Goel et al., 2021).

**Behenic acid (2.12):** White powder; 1.5 gm; $^1H$ NMR (500 MHz, $CDCl_3$) δ 2.38 - 2.35 (t, 2H), 1.68 – 1.62 (dt, 2H), 1.32 – 1.28 (m, 36H), 0.91-0.89 (t, 3H); $^{13}C$ NMR (125 MHz, $CDCl_3$) δ 179.4, 33.9, 31.9, 29.7, 29.6, 29.4, 29.3, 29.2, 29.1, 24.7, 22.7, 14.1 (Zheng et al., 2004).

**Behenyl alcohol (2.13)**: White waxy solid; 0.8 gm; $^1H$ NMR (500 MHz, $CDCl_3$) δ 3.67-3.65 (t, 2H), 1.61 – 1.56 (m, 2H), 1.33 – 1.27 (m, 38H), 0.91-0.88 (t, 3H); $^{13}C$ NMR (125 MHz, $CDCl_3$) δ 63.1, 32.8, 31.9, 29.7, 29.7, 29.6, 29.5, 29.4, 25.7, 22.7, 14.2 (Ajithabai et al., 2011).

**Tetracosyl ferulate (2.14):** White waxy solid; 0.5 gm; $^1H$ NMR (500 MHz, $CDCl_3$) δ 7.63 (d, *J* = 15.9 Hz, 1H), 7.09 (dd, *J* = 8.2, 1.4 Hz, 1H), 7.06 (s, 1H), 6.94 (d, *J* = 8.2 Hz, 1H), 6.31 (d, *J* = 15.9 Hz, 1H), 4.21 (t, *J* = 6.7 Hz, 2H), 3.95 (s, 3H), 1.75 – 1.68 (m, 2H), 1.45 – 1.38 (m, 2H), 1.29 (m, 40H), 0.90 (t, *J* = 6.9 Hz, 3H). $^{13}C$ NMR (125 MHz, $CDCl_3$)

δ 167.4, 147.9, 146.7, 144.6, 127.1, 123.1, 115.6, 114.7, 109.2, 64.6, 55.9, 31.9, 29.7, 29.7, 29.6, 29.6, 29.4, 29.3, 28.8, 26.0, 22.7, 14.2 (Xiang et al., 2008).

**Stigmasterol (2.15):** See Appendix (Forgo and Kövér, 2004).

**β-sitosterol (2.16):** See Appendix (Ododo et al., 2016).

**7,3',5'-tri-*O*-methyltricetin (2.17):** Yellow needles; 56 mg; $^{1}$H NMR (500 MHz, $CDCl_3$) δ 12.74 (s, 1H), 7.20 (d, 1H), 6.98 (d, 1H), 6.60 (s, 1H), 6.51 (d, 1H), 6.40 (d, 1H), 5.99 (s, 1H), 4.00 (d, 6H), 3.91 (s, 3H); $^{13}$C NMR (125 MHz, $CDCl_3$) δ 182.4, 165.6, 163.6, 162.2, 157.7, 152.5, 149.6, 138.6, 126.9, 106.7, 105.6, 105.6, 102.4, 98.2, 92.7, 61.2, 56.1, 55.8 (Zahir et al., 1996).

**Apigenin (2.18):** See Appendix (Owen et al., 2003).

### 2.3.4. Cell line and cell culture

All the cell lines were procured from NCI-Bethesda, USA and cultured as per the protocol provided. Cells were grown in a $CO_2$ incubator (Esco) at 37 °C with 98% humidity and 5% $CO_2$ gas environment.

### 2.3.5. Cell viability assay

The MTT colorimetric assays (an assay which measures color changes) was used for measuring the activity of enzymes that reduce MTT to formazan, giving a purple color. Yellow MTT (3-(4,5-Dimethylthiazol-2-yl)-2,5-diphenyltetrazolium bromide, a tetrazole) is reduced to purple formazan in living cells. A solubilization solution (usually either dimethyl sulfoxide, an acidified ethanol solution, or a solution of the detergent sodium dodecyl sulfate in diluted hydrochloric acid) was added to dissolve the insoluble purple formazan product into a colored solution. The absorbance of this colored solution was quantified by measuring at a certain wavelength (usually between 500 and 600 nm)

by a spectrophotometer. The absorption maximum is dependent on the solvent employed (Guru et al., 2015).

### 2.3.6. Fluorescence microscopy

A549 cells were treated with indicated concentrations of ipomone for 48 h. After treatment cells were collected, washed with PBS twice, and fixed in 400 µl cold acetic acid: methanol (1:3, v/v) overnight at 4 °C. The next day, cells were washed and dispensed in 50 µl of fixing solution. The cells were then spread on a clean slide and dried overnight at room temperature. Cells were stained with DAPI (5µg/ml in 0.01 M citric acid and 0.45 M disodium phosphate containing 0.05% Tween 20) for 30 min at room temperature and subsequently, the slides were washed with distilled water followed by washing with PBS. While wet, 40 µl of mounting fluid (PBS: glycerol, 1:1) was poured over the slide and covered with a glass coverslip and sealed. Cells were observed under a microscope for any nuclear morphological changes that occur during apoptosis. For phase-contrast microscopy, cells were simply photographed using a microscope after treatment (Guru et al., 2015).

### 2.3.7. Acridine orange staining

The induction of autophagy was analyzed by staining cells with acridine orange (AO) as described earlier (Kumar et al., 2013). Briefly, $0.5X10^6$ cells were seeded in a six-well plate and treated with ipomone for 48 h. Cells were incubated with 1 mg/ml AO for 15 min before the termination of the experiment and were washed with PBS before analyzing on a fluorescence microscope.

### 2.3.8. Preparation of whole-cell lysates for immunoblotting

Cells (2 × $10^6$/well) were seeded and treated with different concentrations of ipomone. A549 cells were treated with 10, 30, and 50µg/ml concentrations of ipomone for 48 h. After 48 h treatment, the cells were harvested and washed with cold PBS. The PBS was decanted, and the pellets resuspended in appropriate volumes of cold RIPA lysis buffer, freshly supplemented with 1% (v/v) eukaryotic protease inhibitor cocktail for 45 minutes and vortexed at 10 minutes intervals while maintaining on ice. The cell lysate was cleared by centrifugation at 14,000 g at 4°C for 15 minutes. The supernatant was transferred to a new tube and used as whole-cell lysates for western blot analysis for the expression status of various proteins.

### 2.3.9. Molecular docking

Molecular docking studies were performed using AutoDock 4.2 to deepen the understanding of the molecular interaction between ligand and proteins viz. caspase-3 (PDB id. 3KJF), p110α (PDB id. 5DXT) and PARP-1 (PDB id. 6I8T) (Morris et al., 2009). The crystal structures were obtained from the protein data bank (https://www.rcsb.org/). The correct protonation state to the residues was assigned using the pdb2pqr web server. All the water molecules, ligands, and ions were removed. Non-polar hydrogen atoms were removed and gasteiger charges were added using M.G.L Tools 1.5.6. AutoDock employs Autogrid4 to compute maps. The active site of the protein was determined using the PLIP web server (https://projects.biotec.tu-dresden.de/plip-web/plip) (Salentin et al., 2015). The docking study was performed using Lamarckian Genetic Algorithm (LGA). The docking was performed with 100 runs, 150 population size, 27,000 number of generations, and 2,500,000 number of energy evaluation. It employs a 'semiempirical free energy force field' to evaluate conformations

at the time of docking simulation. The docked pose was visualized by Maestro for studying interactions.

### 2.3.10. Procedure for the synthesis of ipomone (2.11)

In a round bottom flask containing 2 ml of methanol, gibberellic acid (346 mg, 1.0 mmol) and iodine (126 mg, 1.0 mmol) were added subsequently. The reaction mixture was stirred at 50 $^{o}$C for 2 hours and its progress was monitored by TLC. After completion, the reaction mixture was cooled to room temperature, diluted with a saturated solution of sodium thiosulfate (50 mL) to remove the unreacted iodine and colored impurities. Then the mixture was partitioned with ethyl acetate and the organic layer was collected and dried over anhydrous $Na_2SO_4$ and concentrated under reduced pressure. Finally, the crude product was purified by silica gel column chromatography using hexane and ethyl acetate.

### 2.3.11. Procedure for the synthesis of compounds 2.19 and 2.20

Gibberellic acid (346 mg, 1.0 mmol) was dissolved in 2 ml of respective solvent (methanol for **2.19**, and ethanol for **2.20**). To this iodine (507.6 mg, 2 mmol) was added. The reaction flask was stirred at 50 °C for 4 hrs. The reaction was monitored over time via TLC. After reaction completion, reaction was quenched by the addition of 50 ml of ethyl acetate and washed with 3 × 50 ml of saturated sodium thiosulfate solution to remove the residual iodine. The organic layer was dried over anhydrous $Na_2SO_4$ and concentrated via rotary evaporation. Finally, the crude product was purified by silica gel column chromatography using hexane and ethyl acetate.

**Methyl-(7S,9aS,10R)-7-(iodomethyl)-1-methyl-8-oxo-6,8,9,10-tetrahydro-7H-7,9a-methanobenzo[a]azulene-10-carboxylate (2.19):** White crystalline solid; Yield: 90 %; m.p. 146-150 °C (uncorrected); $^{1}$H NMR (500 MHz, $CDCl_3$) δ 7.32 (d, $J$ = 7.6 Hz, 1H), 7.25 (t, $J$ = 7.5 Hz, 1H), 7.12 (d, $J$ = 7.4 Hz, 1H), 5.91 (t, $J$ = 3.5 Hz, 1H), 4.07 (s, 1H),

3.75 (s, 3H), 3.51 (d, *J* = 10.3 Hz, 1H), 3.34 (d, *J* = 10.4 Hz, 1H), 2.65 (dd, *J* = 18.1, 3.0 Hz, 1H), 2.57 (dd, *J* = 17.3, 3.5 Hz, 1H), 2.46 (d, *J* = 17.4 Hz, 1H), 2.39 (d, *J* = 10.9 Hz, 1H), 2.30 (dd, *J* = 18.3, 4.1 Hz, 1H), 2.27 (s, 3H), 2.09 – 2.05 (m, 1H); $^{13}$C NMR (125 MHz, $CDCl_3$) δ 215.4, 172.0, 149.1, 139.9, 138.1, 135.2, 130.0, 128.8, 118.8, 113.1, 55.0, 54.9, 53.7, 52.1, 48.5, 40.9, 37.9, 18.6, 10.4; HRMS *m/z* 423.0434 $[M+H]^+$ (calcd for $C_{19}H_{20}IO_3^+$, 423.0452)

**Ethyl-(7S,9aS,10R)-7-(iodomethyl)-1-methyl-8-oxo-6,8,9,10-tetrahydro-7H-7,9a-methanobenzo[a]azulene-10-carboxylate (2.20):** White crystalline solid; Yield: 90 %; m.p. 141-144 °C (uncorrected); $^1$H NMR (500 MHz, $CDCl_3$) δ 7.31 (d, *J* = 7.6 Hz, 1H), 7.24 (t, *J* = 7.5 Hz, 1H), 7.11 (d, *J* = 7.4 Hz, 1H), 5.90 (t, *J* = 3.5 Hz, 1H), 4.28 – 4.24 (m, 1H), 4.24 – 4.20 (m, 1H), 4.04 (s, 1H), 3.51 (d, *J* = 10.3 Hz, 1H), 3.35 (s, 1H), 2.65 (dd, *J* = 18.1, 3.0 Hz, 1H), 2.57 (dd, *J* = 17.3, 3.4 Hz, 1H), 2.46 (d, *J* = 17.4 Hz, 1H), 2.40 (d, *J* = 11.0 Hz, 1H), 2.31 (d, *J* = 3.9 Hz, 1H), 2.27 (s, 3H), 2.11 (dd, *J* = 11.0, 3.4 Hz, 1H), 1.30 (t, *J* = 7.1 Hz, 3H); $^{13}$C NMR (125 MHz, $CDCl_3$) δ 215.5, 171.4, 149.2, 140.1, 138.1, 135.2, 130.0, 128.7, 118.8, 113.0, 61.1, 55.1, 54.9, 53.6, 48.5, 41.1, 37.9, 18.6, 14.5, 10.5; HRMS *m/z* 437.0615 $[M+H]^+$ (calcd for $C_{20}H_{22}IO_3^+$, 437.0608).